indices.

(ii) For the special case $\epsilon_1 = 0$ no tricritical point occurs, in contrast to the case $\epsilon_2 = 0$. The exceptional behavior of the thermodynamical quantities in the critical point $Q(\mu_c, 0, T_c)$ is explained by the fact that here Γ is parallel to the h axis.

(iii) The model may be used for several different physical systems. For instance, if $S_i = 0$ denotes a vacancy on site i, a *paramagnetic lattice gas* is described. The susceptibility diverges even in the absence of ferromagnetic coupling if a critical point P ($\neq Q$) is approached. The critical exponents of the van der Waals gas for the compressibility and the specific heat coincide with ours.

*Supported by the Schweizerischer Nationalfonds.

[1]Franz Rys, Helv. Phys. Acta 42, 606 (1969).

[2]A. Hintermann and Franz Rys, Helv. Phys. Acta 42, 608 (1969).

[3]A. Hintermann, Diplomarbeit, Eidgenössische Technische Hochschule, Zürich, 1969 (unpublished).

[4]S. Katsura and B. Tsujiyama, in *Proceedings of a Conference on Critical Phenomena*, Natl. Bur. Std. (U. S.) Misc. Publ. 273 (U.S. GPO, Washington, D. C., 1966).

[5]M. Suzuki, B. Tsujiyama, and S. Katsura, J. Math. Phys. 8, 124 (1967).

[6]R. B. Griffiths, Phys. Rev. Letters 24, 715 (1970).

[7]H. W. Cappel, Physica 32, 966 (1966).

[8]J. Oitmaa, Phys. Letters 33A, 230 (1970).

[9]J. Bernasconi, T. Kobine, and Franz Rys (unpublished).

[10]R. B. Griffiths, Physica 33, 689 (1967).

[11]M. E. Fisher, Phys. Rev. 176, 257 (1968).

[12]R. B. Griffiths and J. C. Wheeler, Phys. Rev. A 2, 1047 (1970).

[13]W. F. Saam, Phys. Rev. A 2, 1461 (1970).

PHYSICAL REVIEW B VOLUME 4, NUMBER 9 1 NOVEMBER 1971

Neutron Orbital Cross Section for a Tight-Binding Model of Paramagnetic Nickel

S. W. Lovesey*
Solid State Division, Oak Ridge National Laboratory, Oak Ridge, Tennessee 37830

and

C. G. Windsor
Materials Physics Division, Atomic Energy Research Establishment, Harwell, Berkshire, England

(Received 5 February 1971)

The orbital contribution to the magnetic partial differential neutron cross section is calculated for a realistic band model of paramagnetic nickel within the tight-binding scheme. The orbital contribution is generally less than one-quarter that of the spin contribution in an energy range up to ~ 0.15 eV. At higher energies it exceeds the spin contribution and should be observable.

I. INTRODUCTION

In the past few years there have been several theoretical and experimental studies aimed at understanding the generalized electron-spin susceptibility $\chi_s(\vec{\kappa}, \omega)$ of magnetic metals.[1-4] $\chi_s(\vec{\kappa}, \omega)$ measures the response of electrons to an external perturbation, of frequency ω and wave vector $\vec{\kappa}$, that couples to their spin; i.e., it describes electron-spin dynamics. Efficient and accurate band-structure calculations have made realistic calculations of χ_s possible. This work has been stimulated by experimental studies, especially thermal neutron scattering experiments.

The neutron-electron interaction evaluated to leading order in the reciprocal of the neutron mass is the sum of two terms,[5] the spin and orbital interactions. The contribution to the neutron cross section from the former is simply related to $\chi_s(\vec{\kappa}, \omega)$. For small scattering wave vectors, Elliott[1] has argued that the matrix element of the orbital interaction operator is a factor m_e/m^* smaller than that of the spin interaction, and it has been assumed to be negligible in experimental analysis. Since fine detail can be measured by neutron scattering, and measurements are not restricted to small wave vectors, the orbital contribution to the neutron cross section now warrants a more complete study. As a first step we have calculated the orbital contribution to the magnetic neutron cross section for a tight-binding model of paramagnetic nickel and compared it with the spin contribution. The latter dominates for small $\vec{\kappa}$ and ω. The two contributions become comparable for $\hbar\omega \sim 0.15$ eV

and the orbital contribution is the larger at higher energies. For example, in the two cases $\vec{\kappa} \sim 0$ and $\vec{\kappa} \sim$ zone boundary, the magnetic scattering comes solely from the orbital interaction for energies exceeding 0.2 and 2 eV, respectively, and should be observable.

The static orbital susceptibility for electrons in a solid, in the absence of many-body effects, has been studied by many authors,[6] but detailed numerical calculations have been made only recently.[7] The corresponding wave-vector-dependent orbital susceptibility has been studied by Hebborn and March.[2,8] Szabo[9] and Schneider[10] have evaluated the generalized orbital susceptibility for a free-electron gas, and this diverges for small $|\vec{\kappa}|$ as $|\vec{\kappa}|^{-2}$. The tight-binding model is more appropriate for a transition metal, and for this model the orbital cross section is finite for zero scattering vector.[11]

In Sec. II an expression for the orbital contribution to the partial differential cross section is derived for a tight-binding model of paramagnetic nickel. The numerical evaluation of the contribution parallels that used previously to study χ_s, and is described briefly in Sec. III. A detailed comparison between the spin and orbital contributions is given in Sec. IV together with our conclusions.

II. THEORY

The partial differential magnetic cross section for unpolarized neutrons is[12]

$$\frac{d^2\sigma}{d\Omega dE'} = \left(\frac{E'}{E}\right)^{1/2}\left(\frac{\gamma e^2}{m_e c^2}\right)^2 \times \frac{1}{2\pi\hbar}\int_{-\infty}^{\infty} dt\, e^{-i\omega t}\langle\{\vec{\mathfrak{D}}^{(\perp)}(0)\}^{\dagger}\cdot\vec{\mathfrak{D}}^{(\perp)}(t)\rangle . \quad (1)$$

In this expression the initial and scattered neutron energies are denoted by E and E', $\hbar\omega = E - E'$, and the interaction constant $(\gamma e^2/m_e c^2)^2 = 0.292$ b. The magnetic interaction operator $\vec{\mathfrak{D}}^{(\perp)}$ that appears in correlation function in (1) is[5]

$$\vec{\mathfrak{D}}^{(\perp)} = \vec{\mathfrak{D}}_s^{(\perp)} + \vec{\mathfrak{D}}_L^{(\perp)} = |\vec{\kappa}|^{-2}\sum_\nu e^{i\vec{\kappa}\cdot\vec{r}_\nu}\{\vec{\kappa}\times(\vec{s}_\nu\times\vec{\kappa}) - i(\vec{\kappa}\times\vec{p}_\nu)/\hbar\} , \quad (2)$$

where $\vec{r}_\nu$, $\vec{s}_\nu$, and $\vec{p}_\nu$ are the position vector and spin and linear momentum operators, respectively, of the νth magnetic electron.

Elliott[1] has studied the cross section (1) for Bloch electrons in the absence of many-body interactions. As noted in Sec. I, he argued that for small $\vec{\kappa}$ and narrow bands the orbital contribution is negligible.

The calculation of the orbital contribution to the cross section (1) is conveniently made by transforming to a second-quantized representation for $\vec{\mathfrak{D}}_L^{(\perp)}$, namely,

$$\vec{\mathfrak{D}}_L^{(\perp)} = -|\vec{\kappa}|^{-2}\sum_{\vec{k},\vec{k}'}\sum_{\lambda,\lambda'}\sum_{\sigma,\sigma'} c^{\dagger}_{\vec{k}'\lambda'\sigma'} c_{\vec{k}\lambda\sigma}\delta_{\sigma,\sigma'} \times \int d\vec{r}\,\psi^{*}_{\vec{k}'\lambda'}(\vec{r})\, e^{i\vec{\kappa}\cdot\vec{r}}\{\vec{\kappa}\times\vec{\nabla}\}\psi_{\vec{k}\lambda}(\vec{r}) . \quad (3)$$

Here $\psi_{\vec{k}\lambda}(\vec{r})$ is a Bloch wave function of wave vector $\vec{k}$ and band λ, and $c_{\vec{k}\lambda\sigma}$ and $c^{\dagger}_{\vec{k}\lambda\sigma}$ are the appropriate Fermi annihilation and creation operators for electrons with spin σ. For a tight-binding model,[13]

$$\psi_{\vec{k}\lambda}(\vec{r}) = \frac{1}{N^{1/2}}\sum_{\vec{l},m} a^m_\lambda(\vec{k}) e^{i\vec{k}\cdot\vec{l}}\,\phi_m(\vec{r}-\vec{l}) , \quad (4)$$

where $\phi_m(\vec{r}-\vec{l})$ is the atomic wave function with magnetic quantum number m centered at the lattice site defined by the vector $\vec{l}$, and $a^m_\lambda(\vec{k})$ are the eigenfunctions of the Fourier transform of the matrix elements of the one-electron Hamiltonian. The matrix element in (3) is evaluated with the Bloch functions (4) and the assumption that integrals involving ϕ's centered on different atomic sites can be neglected. We thereby obtain

$$\vec{\mathfrak{D}}_L^{(\perp)} = -|\vec{\kappa}|^{-2}\sum_{\vec{k},\vec{k}'}\sum_{\lambda\lambda'}\sum_{\sigma} c^{\dagger}_{\vec{k}'\lambda'\sigma} c_{\vec{k}\lambda\sigma} \times \frac{1}{N}\sum_{\vec{l}} e^{i(\vec{\kappa}+\vec{k}-\vec{k}')\cdot\vec{l}}\,\vec{A}^{\lambda\lambda'}(\vec{k},\vec{k}') , \quad (5)$$

where

$$\vec{A}^{\lambda\lambda'}(\vec{k},\vec{k}') = \sum_{m,m'} a^{m'}_\lambda(\vec{k})\{a^m_{\lambda'}(\vec{k}')\}^{*}\int d\vec{r}\,\phi^{*}_m(\vec{r})\, e^{i\vec{\kappa}\cdot\vec{r}}\{\vec{\kappa}\times\vec{\nabla}\}\phi_{m'}(\vec{r}) . \quad (6)$$

The atomic wave function ϕ_m is the product of a radial wave function $f(r)$ and a spherical harmonic $Y^l_m(\vec{r})$. The matrix element in (6), which we henceforth denote by $\vec{\Gamma}^{mm'}$, can be evaluated exactly. Following Johnston,[14] we find for the qth spherical component of $\vec{\Gamma}^{mm'}$ the result

$$\Gamma^{mm'}_q = -|\vec{\kappa}|^2(\tfrac{4}{3}\pi)^{1/2}(2l+1)^{3/2}\sum_{KQ}\sum_{K'Q'} i^{K'+1}\,Y^K_Q(\vec{\kappa}) \times[\langle j_{K'-1}\rangle + \langle j_{K'+1}\rangle]\,T(K,K')A(K',K',l) \times (K'Q'lm\,|\,l'm')\,(KQK'Q'\,|\,1q) . \quad (7)$$

In this expression the integer $K' = 1, 3, \ldots, 2l-1$ and

$$T(K,K') = (K')^{1/2} \quad \text{if } K = K'+1$$
$$= (K'+1)^{1/2} \quad \text{if } K = K'-1$$
$$= 0 \quad \text{otherwise} . \quad (8)$$

The radial integrals $\langle j_K \rangle$ are defined by

$$\langle j_K \rangle = \int_0^\infty dr\, r^2 f^2(r) j_K(\kappa r) , \tag{9}$$

where $j_K(\kappa r)$ is a spherical Bessel function of order K. Finally,

$$A(K', K', l) = (-1)^{l+1} \left[\frac{l(2l-1)}{2l+1} \right]^{1/2} \times \begin{pmatrix} l & K' & l-1 \\ 0 & 0 & 0 \end{pmatrix} \begin{Bmatrix} l & 1 & l-1 \\ K' & l & K' \end{Bmatrix} , \tag{10}$$

where the 3-j and 6-j symbols, and also the Clebsch-Gordan coefficients in (7), are defined by Edmonds.[15]

$\Gamma_q^{mm'}$ satisfies two symmetry relationships that are useful in calculations. Since it is the matrix element of a Hermitian operator, we have

$$\Gamma_q^{m'm} = (-1)^q (\Gamma_{-q}^{mm'})^* , \tag{11a}$$

and, secondly, a direct calculation proves that

$$\Gamma_q^{-m',-m} = (-1)^{m+m'+1} \Gamma_q^{mm'} . \tag{11b}$$

Note that $\vec{\Gamma}^{-m,-m} = -\vec{\Gamma}^{mm}$ and $\vec{\Gamma}^{m,-m} = 0$.

By utilizing (11) and

$$a_\lambda^{m\,*}(\vec{k}) = (-1)^m a_\lambda^{-m}(\vec{k}) , \tag{12}$$

the 25 terms in $\vec{A}^{\lambda\lambda'}$, Eq. (6), can be reduced to

$$\begin{aligned} \vec{A}^{\lambda\lambda'} = {} & \vec{\Gamma}^{22}\, 2i\, \mathrm{Im}(a_\lambda^{2\,*} a_{\lambda'}^2) \\ & + \vec{\Gamma}^{11}\, 2i\, \mathrm{Im}(a_\lambda^{1\,*} a_{\lambda'}^1) + \vec{\Gamma}^{21}(a_\lambda^{2\,*} a_{\lambda'}^1 - a_\lambda^1 a_{\lambda'}^{2\,*}) \\ & + \vec{\Gamma}^{20}(a_\lambda^{2\,*} a_{\lambda'}^0 - a_\lambda^0 a_{\lambda'}^{2\,*}) + \vec{\Gamma}^{2,-1}(a_\lambda^{1\,*} a_{\lambda'}^{2\,*} - a_\lambda^{2\,*} a_{\lambda'}^{1\,*}) \\ & + \vec{\Gamma}^{12}(a_\lambda^{1\,*} a_{\lambda'}^2 - a_\lambda^2 a_{\lambda'}^{1\,*}) + \vec{\Gamma}^{10}(a_\lambda^{1\,*} a_{\lambda'}^0 - a_\lambda^0 a_{\lambda'}^{1\,*}) \\ & + \vec{\Gamma}^{02}(a_\lambda^0 a_{\lambda'}^2 - a_\lambda^2 a_{\lambda'}^0) + \vec{\Gamma}^{01}(a_\lambda^0 a_{\lambda'}^1 - a_\lambda^1 a_{\lambda'}^0) \\ & + \vec{\Gamma}^{-1,2}(a_\lambda^2 a_{\lambda'}^1 - a_\lambda^1 a_{\lambda'}^2) . \end{aligned} \tag{13}$$

From this expression note that $\vec{A}^{\lambda\lambda'} = -\vec{A}^{\lambda'\lambda}$.

The relative magnitude of the various terms in (7) is determined by the radial integrals $\langle j_K \rangle$. Only $\langle j_0 \rangle$ is finite for zero wave vector, and to a good approximation we can neglect the term coming from $K' = 3$. The coefficient of $\langle j_2 \rangle$ in this term is on average about $\frac{1}{5}$ that coming from the $K' = 1$ term. In this approximation

$$\vec{\mathfrak{D}}_L^{(1)} \simeq [\langle j_0 \rangle + \langle j_2 \rangle] \sum_{\vec{k},\vec{k}'} \sum_{\lambda,\lambda'} \sum_\sigma c_{\vec{k}'\lambda\sigma}^\dagger c_{\vec{k}\lambda'\sigma} \times \left\{ \frac{1}{N} \sum_{\vec{l}} e^{i(\vec{\kappa}+\vec{k}-\vec{k}')\cdot\vec{l}} \right\} \hat{\vec{A}}^{\lambda\lambda'}(\vec{k}, \vec{k}') , \tag{14}$$

and the reduced $\hat{\vec{A}}^{\lambda\lambda'}$ in (14) is calculated from (13) neglecting $\vec{\Gamma}^{20}$, $\vec{\Gamma}^{2,-1}$, $\vec{\Gamma}^{02}$, and $\vec{\Gamma}^{-1,2}$, and with the remaining $\vec{\Gamma}^{mm'}$ terms replaced by either

$$\hat{\Gamma}_q^{mm} = \tfrac{1}{3} m \{ -\delta_{q,0} + Y_q^2(\vec{\kappa}) [\tfrac{1}{5}\pi(4-q^2)]^{1/2} \} \tag{15a}$$

or

$$\hat{\Gamma}_q^{m+1,m} = \tfrac{1}{6} [(2-m)(3+m)]^{1/2} \times \{ \delta_{1,q}\sqrt{2} + Y_{q-1}^2(\vec{\kappa}) [\tfrac{1}{5}\pi(2-q)(3-q)]^{1/2} \} . \tag{15b}$$

Using the spherical harmonics as defined by Edmonds,[15] we obtain the values shown in Table I for the $\hat{\Gamma}_q^{m'm}$ as functions of the polar angles θ and ϕ of $\vec{\kappa}$ with respect to the quantization axes.

The remaining terms in Eq. (13) may be simplified by writing the atomic wave-function coefficients $a_\lambda^m(\vec{k})$ in terms of the coefficients of the irreducible representations of the continuous group $l = 2$ in cubic symmetry. These coefficients, which we denote by $C_\mu^\lambda(\vec{k})$, are purely real and are related to the $a_\lambda^m(\vec{k})$ by

$$\begin{aligned} a_\lambda^2 &= (1/\sqrt{2})(-iC_{xy}^\lambda + C_{x^2-y^2}^\lambda) , \\ a_\lambda^1 &= (1/\sqrt{2})(iC_{yz}^\lambda - C_{zx}^\lambda) , \\ a_\lambda^0 &= C_{3z^2-r^2}^\lambda . \end{aligned} \tag{16}$$

We then have

$$\hat{A}_q^{\lambda\lambda'} = \hat{\Gamma}_q^{22} C_1 + \hat{\Gamma}_q^{11} C_2 + \hat{\Gamma}_q^{21}(C_3 + iD_3) + \hat{\Gamma}_q^{12}(-C_3 + iD_3) + \hat{\Gamma}_q^{10}(C_4 + iD_4) + \hat{\Gamma}_q^{01}(-C_4 + iD_4) , \tag{17}$$

where

$$\begin{aligned} C_1 &= -C_{xy}^\lambda C_{x^2-y^2}^{\lambda'} + C_{x^2-y^2}^\lambda C_{xy}^{\lambda'} , \\ C_2 &= -C_{yz}^\lambda C_{zx}^{\lambda'} + C_{zx}^\lambda C_{yz}^{\lambda'} , \\ C_3 &= \tfrac{1}{2}(-C_{xy}^\lambda C_{yz}^{\lambda'} - C_{x^2-y^2}^\lambda C_{zx}^{\lambda'} + C_{yz}^\lambda C_{xy}^{\lambda'} + C_{zx}^\lambda C_{x^2-y^2}^{\lambda'}) , \\ D_3 &= \tfrac{1}{2}(-C_{xy}^\lambda C_{zx}^{\lambda'} - C_{yz}^\lambda C_{x^2-y^2}^{\lambda'} + C_{x^2-y^2}^\lambda C_{yz}^{\lambda'} + C_{zx}^\lambda C_{xy}^{\lambda'}) , \\ C_4 &= (1/\sqrt{2})(C_{3z^2-r^2}^\lambda C_{zx}^{\lambda'} - C_{zx}^\lambda C_{3z^2-r^2}^{\lambda'}) , \\ D_4 &= (1/\sqrt{2})(C_{3z^2-r^2}^\lambda C_{yz}^{\lambda'} - C_{yz}^\lambda C_{3z^2-r^2}^{\lambda'}) . \end{aligned} \tag{18}$$

Using expression (14) for $\mathfrak{D}_L^{(1)}$, the correlation function in (1) for noninteracting electrons is [the cross term in (1) involving $\mathfrak{D}_s^{(1)}$ and $\mathfrak{D}_L^{(1)}$ is zero]

TABLE I. Values of $\hat{\Gamma}_q^{m'm}$.

q	0	1	−1
$\hat{\Gamma}_q^{22}$	$-\sin^2\theta$	$-(1/\sqrt{2})\sin\theta\cos\theta e^{i\phi}$	$(1/\sqrt{2})\cos\theta\sin\theta e^{i\phi}$
$\hat{\Gamma}_q^{11}$	$-\frac{1}{2}\sin^2\theta$	$-(1/2\sqrt{2})\sin\theta\cos\theta e^{i\phi}$	$(1/2\sqrt{2})\cos\theta\sin\theta e^{-i\phi}$
$\hat{\Gamma}_q^{21}$	$\frac{1}{2}\cos\theta\sin\theta e^{-i\phi}$	$(1/2\sqrt{2})(1+\cos^2\theta)$	$(1/2\sqrt{2})\sin^2\theta e^{-2i\phi}$
$\hat{\Gamma}_q^{12}$	$\frac{1}{2}\cos\theta\sin\theta e^{i\phi}$	$-(1/2\sqrt{2})(1+\cos^2\theta)$	$-(1/2\sqrt{2})\sin^2\theta e^{2i\phi}$
$\hat{\Gamma}_q^{10}$	$(\sqrt{\frac{3}{8}})\cos\theta\sin\theta e^{-i\phi}$	$(\sqrt{\frac{3}{16}})(1+\cos^2\theta)$	$(\sqrt{\frac{3}{16}})\sin^2\theta e^{-2i\phi}$
$\hat{\Gamma}_q^{01}$	$(\sqrt{\frac{3}{8}})\cos\theta\sin\theta e^{i\phi}$	$-(\sqrt{\frac{3}{16}})(1+\cos^2\theta)$	$-(\sqrt{\frac{3}{16}})\sin^2\theta e^{2i\phi}$

$$\frac{1}{2\pi\hbar}\int_{-\infty}^{\infty} dt\, e^{-i\omega t}\langle\{\vec{\mathfrak{D}}_L^{(1)}(0)\}^{\dagger}\cdot\vec{\mathfrak{D}}_L^{(1)}(t)\rangle$$

$$=\frac{4}{\pi}\frac{[\langle j_0\rangle+\langle j_2\rangle]^2}{1-e^{(-\hbar\omega\beta)}}\mathrm{Im}\chi_L^0(\vec{\kappa},\omega)\,, \qquad (19)$$

where the imaginary part of the noninteracting orbital susceptibility χ_L^0 is

$$\mathrm{Im}\chi_L^0(\vec{\kappa},\omega)=-\frac{\pi}{2}\sum_{\vec{k},\lambda,\lambda'}(f_{\vec{k}+\vec{\kappa}\lambda}-f_{\vec{k}\lambda'})\left|\hat{A}^{\lambda\lambda'}(\vec{k},\vec{k}+\vec{\kappa})\right|^2$$
$$\times\delta(\hbar\omega+\mathcal{E}_{\vec{k}\lambda'}-\mathcal{E}_{\vec{k}+\vec{\kappa}\lambda})\,. \qquad (20)$$

In (17), $f_{\vec{k}\lambda}$ is the Fermi-Dirac function for the electron band energy $\mathcal{E}_{\vec{k}\lambda}$ and temperature $T=1/k_B\beta$. The expressions for $|\hat{A}_q^{\lambda\lambda'}(\vec{k},\vec{k}+\vec{\kappa})|^2$ can be evaluated in terms of the coefficients given above in Eqs. (17) and (18). We obtain

$$\begin{aligned}
|\hat{A}_0^{\lambda\lambda'}|^2&=\{\sin^2\theta\,P\}^2+\{\cos\theta\sin\theta\,(\cos\phi\,R-\sin\phi\,Q)\}^2\,,\\
|\hat{A}_{+1}^{\lambda\lambda'}|^2&=\tfrac{1}{2}\{-\sin\theta\cos\theta\cos\phi\;P+(1+\cos^2\theta)Q\}^2\,,\\
|\hat{A}_{-1}^{\lambda\lambda'}|^2&=\tfrac{1}{2}\{\sin\theta\cos\theta\cos\phi\,P\\
&\quad+\sin^2\theta\cos2\phi\,Q+\sin^2\theta\sin2\phi\,R\}^2\,,
\end{aligned} \qquad (21)$$

where

$$\begin{aligned}
P&=C_1+\tfrac{1}{2}C_2\,,\\
Q&=C_3+(\sqrt{\tfrac{3}{2}})C_4\,,\\
R&=D_3+(\sqrt{\tfrac{3}{2}})D_4\,.
\end{aligned} \qquad (22)$$

For the spin contribution, the corresponding expression is

$$\frac{1}{2\pi\hbar}\int_{-\infty}^{\infty} dt\, e^{-i\omega t}\langle\{\vec{\mathfrak{D}}_s^{(1)}(0)\}^{\dagger}\cdot\vec{\mathfrak{D}}_s^{(1)}(t)\rangle$$

$$=\frac{2}{\pi}\frac{|F(\vec{\kappa})|^2}{1-e^{-\hbar\omega\beta}}\mathrm{Im}\chi_s(\vec{\kappa},\omega)=2\left|F(\vec{\kappa})\right|^2 S_s(\vec{\kappa},\omega)\,. \qquad (23)$$

Here $F(\vec{\kappa})$ is the atomic form factor and $\chi_s(\vec{\kappa},\omega)$ has the same structure as (20) with $|\hat{A}^{\lambda\lambda'}(\vec{k},\vec{k}+\vec{\kappa})|^2$ in (20) replaced by

$$\left|\sum_\mu C_\mu^\lambda(\vec{k})C_\mu^{\lambda'}(\vec{k}+\vec{\kappa})\right|^2\,. \qquad (24)$$

III. NUMERICAL CALCULATION

Over the last few few years considerable experience has been gained in the calculation of the spin susceptibility by evaluation of the Lindhard expression (20) with the spin matrix element (24).[4] We have used similar methods to evaluate the orbital susceptibility for a realistic band model of nickel, using the orbital matrix elements of Eq. (21).

The summation over electron wave vectors $\vec{k}$ within the Brillouin zone is performed by setting up a simple cubic mesh in the irreducible $\frac{1}{48}$ of the Brillouin zone, and a summation over these points is followed by a summation over the various inequivalent irreducible zones. The energy δ function occurring in the imaginary part of the susceptibility is used to construct a histogram with ω as parameter, and in this way $\chi_L^0(\vec{\kappa},\omega)$ can be calculated for all values of ω with a single summation over $\vec{k}$. Using a histogram spacing in energy of 0.01 eV and with 690 points in the irreducible zone, this method gives a statistical error of order 20% in the imaginary part of the susceptibility, arising from the varying number of points included in each box. This cause of error may be essentially removed by performing an analytic integration within each mesh unit, but we feel that this procedure was not justified in the present case in view of the other uncertainties in the calculation.

The matrix elements (21) of the orbital calculation are more complicated than in the spin case, since they depend explicitly on the polar coordinates θ, ϕ of the scattering vector $\vec{\kappa}$ relative to the quantization axis of the wave functions. This means that for each irreducible $\frac{1}{48}$ part of the zone the orbital matrix element is in general a different function of the wave-function coefficients $C_\mu^\lambda(\vec{k})$. However, when $\vec{\kappa}$ lies along high-symmetry directions in the zone, many of the irreducible zones become equivalent, and even for these the matrix elements reduce to simple functions of the wave-function coefficients, so that little more computing effort is required than in the spin case. In Table II we give the orbital matrix elements $\sum_q|\hat{A}_q^{\lambda\lambda'}|^2$ for the various inequivalent irreducible zones occuring when $\vec{\kappa}$ lies along the [100], [110], and [111] direc-

TABLE II. Orbital matrix elements along high-symmetry directions. The notation used is defined in Eqs. (18) and (21). In each direction there are other inequivalent zones, formed from those shown by inversion about the origin, whose matrix elements have the same form.

Direction	Zone	θ,ϕ	$\sum_q\lvert\hat{A}_q^{\lambda\lambda'}\rvert^2$
[100]	1	0, 0	$2Q^2$
	2	$\frac{1}{2}\pi$, 0	P^2+Q^2
	3	$\frac{1}{2}\pi$, $\frac{1}{2}\pi$	
[110]	1	$\frac{1}{2}\pi$, $\frac{1}{4}\pi$	$P^2+\frac{1}{2}Q^2+\frac{1}{2}R^2$
	2	$\frac{1}{2}\pi$, $\frac{3}{4}\pi$	
	3	$\frac{1}{4}\pi$, $\frac{1}{2}\pi$	$\frac{1}{2}P^2+\frac{3}{2}Q^2$
	4	$\frac{1}{4}\pi$, $\frac{3}{4}\pi$	
	5	$\frac{1}{4}\pi$, 0	$\frac{1}{2}P^2+\frac{5}{4}Q^2+\frac{1}{4}R^2-\frac{1}{2}PQ$
	6	$\frac{1}{4}\pi$, π	$\frac{1}{2}P^2+\frac{5}{4}Q^2+\frac{1}{4}R^2+\frac{1}{2}PQ$
[111]	1	$\cos^{-1}(\sqrt{\frac{2}{3}})$, $\frac{1}{4}\pi$	$\frac{2}{3}P^2+Q^2+\frac{1}{3}R^2+\frac{2}{3}(-RQ-2PQ+2PR)$
	2	$\cos^{-1}(\sqrt{\frac{2}{3}})$, $\frac{3}{4}\pi$	$\frac{2}{3}P^2+Q^2+\frac{1}{3}R^2+\frac{2}{3}(RQ+2PQ+2RP)$
	3	$\cos^{-1}(\sqrt{\frac{2}{3}})$, $\frac{5}{4}\pi$	$\frac{2}{3}P^2+Q^2+\frac{1}{3}R^2+\frac{2}{3}(RQ-2PQ-2RP)$
	4	$\cos^{-1}(\sqrt{\frac{2}{3}})$, $\frac{7}{4}\pi$	$\frac{2}{3}P^2+Q^2+\frac{1}{3}R^2+\frac{2}{3}(-RQ+2PQ+2RP)$

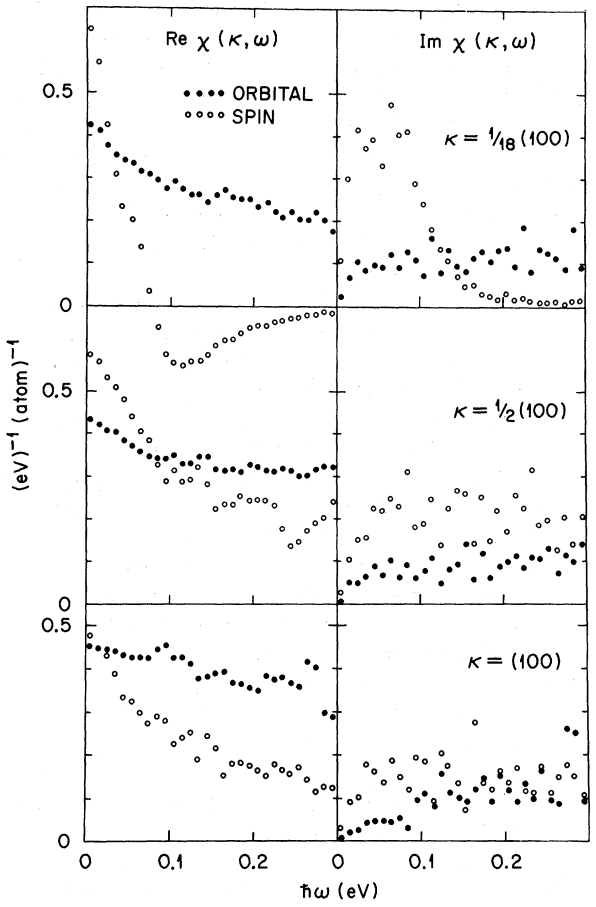

FIG. 1. Real and imaginary parts of the orbital and spin susceptibilities for nickel at $1.6T_c$ calculated by numerical evaluation of the Lindhard summation without including electron interactions. A mesh in reciprocal space of size $2\pi/18a_0$ was used, and the results are shown for $\kappa = \frac{1}{18}$, $\frac{1}{2}$, and 1 times the zone-boundary value $2\pi/a_0$ in the [100] direction.

tions. The sum over the values of $q = 0, +1$, and -1 occurs following the expansion of Eq. (5) into spherical components.

We show in Fig. 1 examples of the real and imaginary parts of the susceptibility $\chi_L^0(\vec{\kappa}, \omega)$ plotted against ω for three values of $\vec{\kappa}$ along the [100] direction for nickel at a temperature of $1.6T_c$. The electron energies $\mathcal{E}_{\vec{k},\lambda}$ are from a $3d$-band structure calculated using a tight-binding approximation interpolation scheme with the parameters given in Table III. The Fermi level was chosen to give a total of 0.6 holes in the band. Further details of the band structure and of the calculation of the spin part (reproduced in Fig. 1 by the open circles) are given in Ref. 4. The orbital susceptibility (shown by the closed circles) is seen to be very different in form from the spin part. From the point of view of current experiments, the imaginary part in the energy range up to 0.1 eV is of most interest, and in this range the orbital contribution is only about one-quarter of the spin contribution. In general the $\vec{\kappa}$ dependence of the orbital susceptibility is very much smaller than in the spin case. In particular, the narrowing of the spin distribution at small $\vec{\kappa}$, shown, for example, at [100] at the top of the figure, is absent in the orbital case. This feature is caused by the wholly intraband nature of the spin matrix elements at small $\vec{\kappa}$. The orbital matrix elements, being entirely interband, show no marked change as $\vec{\kappa}$ goes to zero. The difference in the matrix elements also shows itself very clearly at very large energy transfers beyond the range of Fig. 1. Figure 2 shows an extension of the $\vec{\kappa} \parallel [100]$ imaginary susceptibility curve to cover the much larger energy range up to 4 eV. It is seen that the spin contribution is dominant only in the extreme left at small energies, while from 0.3 to 4 eV the orbital contribution is the larger. In particular, at around 3-eV energy transfers the orbital contribution is dominant. Unfortunately, this energy range is not easily accessible experimentally. The origin of the

TABLE III. Slater-Koster parameters for the band structure used. [The notation is that of J. Slater and G. Koster, Phys. Rev. 94, 1498 (1954).]

$dd\sigma$	−0.4977
$dd\pi$	0.3057
$dd\delta$	−0.0839
$d_0(t_{2g})$	2.4882
$d_0(e_g)$	2.1768

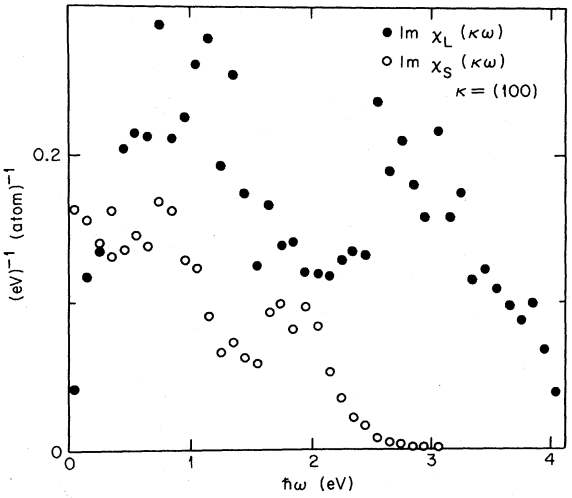

FIG. 2. Imaginary part of the orbital and spin susceptibilities for nickel at the [100] zone boundary, as in the lower portion of Fig. 1, over the full energy range up to 4 eV.

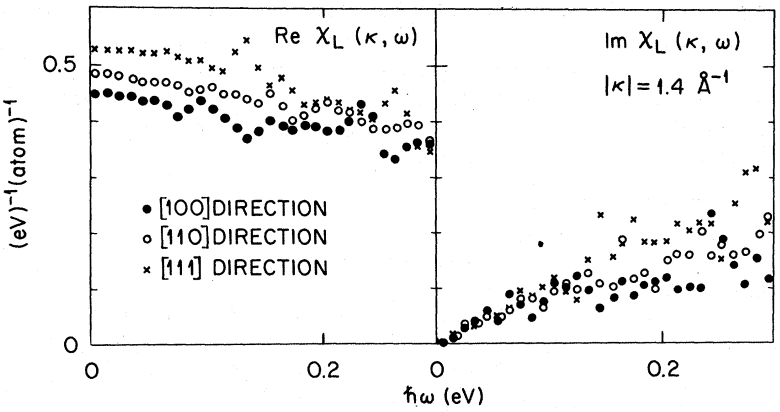

FIG. 3. Anisotropy of the orbital susceptibility for nickel at $1.6T_c$, as illustrated for a value of $|\kappa|$ close to 1.4 Å^{-1} in the three principal directions.

earlier decay of the spin susceptibility with increasing energy has been investigated by examining the individual terms in the Lindhard summation (20). It is found that the electron excitations with energy transfers exceeding 3 eV tend to be from near the bottom of the band structure, which occurs at the point x, to near the top of the band structure, which is in fact also at the point x. The relevant wave functions tend to be nearly orthogonal so that the spin susceptibility, which depends on an overlap-type matrix element, tends to be small. In contrast, the orbital matrix element is composed of sums of terms of the form $C_\mu^\lambda C_{\mu'}^{\lambda'} - C_{\mu'}^\lambda C_\mu^{\lambda'}$, in the notation of (16), which are of order unity for some of the levels involved.

Returning to the real part of the susceptibilities, illustrated in the left-hand side of Fig. 1, it is remarkable that the orbital susceptibility $\mathrm{Re}\chi_L^0(\vec{\kappa},\omega)$ is as much as $\frac{2}{3}$ that of the spin in the static as $\vec{\kappa}$ and ω go to zero, has little $\vec{\kappa}$ dependence, and only modest ω dependence over the range of Fig. 1. These results follow from the presence, discussed in the previous paragraph, of the appreciable imaginary part of the orbital susceptibility extending to high energies. This gives a large contribution to the Kramers-Kronig integral used in evaluating the real part.

The anisotropy of the orbital scattering is shown in Fig. 3 for an intermediate value of the scattering vector of 1.4 Å^{-1}. The magnitude of the anisotropy between the three principal directions is seen to be scarcely above the statistical error at energies below 0.15 eV. Even at higher energies the anisotropy is not appreciably above that observed in the spin susceptibility,[14] and little is seen of the extreme anisotropy evident in the single orbital example treated earlier by the authors.[11]

IV. DISCUSSION

There are several general features of the orbital cross section that are worth explicit mention. First, the orbital interaction operator is independent of the electron spin and hence its contribution to the cross section adds to the longitudinal spin susceptibility. Also, in contrast to the result for a free-electron gas,[9,10] the orbital cross section for the tight-binding model is finite for $|\vec{\kappa}| = 0$. Finally, there are no intraband contributions to the orbital cross section because $\vec{A}^{\lambda\lambda'}$, Eq. (13), is an antisymmetric matrix.

Comparing Eqs. (19) and (23) for the orbital and spin contributions to the cross section, $\langle j_0\rangle + \langle j_2\rangle$ has the role of an orbital form factor. To compare its behavior as a function of $|\vec{\kappa}|$ with the atomic form factor $F(\vec{\kappa})$ we can take the value of $\langle j_0\rangle + \langle j_2\rangle$ calculated by Watson and Freeman[16] and Mook's[17] measurement of $F(\vec{\kappa})$. The comparison shows that they have a similar shape with $\langle j_0\rangle + \langle j_2\rangle$ expanded over $F(\vec{\kappa})$, with the difference at large $|\vec{\kappa}|$ giving an extra factor of 2 in the orbital contribution to the cross section.

Turning to the comparison of the calculated orbital and spin scattering from the point of view of experiment, it is clear that in the region of current neutron experiments, where $\hbar\omega$ is below 0.12 eV, the spin contribution greatly exceeds the orbital. At these low energies the effect of electron interactions is almost certain to increase this disparity. However, for $\hbar\omega \sim 0.15$ eV, the two contributions become comparable and thereafter the spin scattering rapidly decreases. We predict a region with $\vec{\kappa} > 0.2$ Å^{-1} and $\hbar\omega > 0.2$ eV where the orbital scattering will be dominant. To investigate this region experimentally will require good neutron fluxes at very high energies, since the form factor forces the use of high-energy incident and scattered neutron energies.

A possible way of separating out the orbital and spin scattering contributions was suggested by Lowde and Windsor.[4] This involved the use of a magnetic field to rotate the spin directions of the aligned ferromagnetic material relative to the scattering vector. This procedure allows separation

of the parallel and perpendicular scattering components (an inelastic spectrometer employing polarized neutrons may also be used for this purpose). If the assumption is made that at low temperatures, when the spin moment is nearly fully aligned, the spin scattering is confined to the perpendicular component, an estimate can be made of the orbital scattering. In practice this is only an upper limit because of the possibly incomplete magnetization of the sample. However, the magnitude observed of about 0.2 eV^{-1} $atom^{-1}$ at energies below 0.04 eV has the predicted order of magnitude.

---

*Visiting scientist from Atomic Energy Research Establishment, Harwell, Berkshire, England.

[1]R. J. Elliott, Proc. Roy. Soc. (London) A235, 289 (1956).
[2]J. E. Hebborn and N. H. March, Advan. Phys. 19, 175 (1970).
[3]E. D. Thompson, Phys. Rev. Letters 19, 635 (1967); H. A. Mook, R. M. Nicklow, E. D. Thompson, and M. K. Wilkinson, J. Appl. Phys. 40, 1450 (1969); F. M. Mueller and J. W. Garland, Bull. Am. Phys. Soc. 13, 58 (1968).
[4]R. D. Lowde and C. G. Windsor, Advan. Phys. 19, 813 (1970).
[5]O. Halpern and M. H. Johnson, Phys. Rev. 55, 898 (1939).
[6]R. Peierls, Z. Physik 80, 763 (1933); J. E. Hebborn and E. H. Sondheimer, J. Phys. Chem. Solids 13, 105 (1960); H. Fukuyama and R. Kubo, J. Phys. Soc. Japan 27, 604 (1969).
[7]M. Shimizu and Y. Takahashi, Phys. Letters 32A, 164 (1970).
[8]J. E. Hebborn and N. H. March, Phys. Letters 29A, 432 (1969).
[9]N. Szabo, Diploma thesis (ETH Zürich, 1967) (unpublished).
[10]T. Schneider, Solid State Commun. 8, 279 (1970).
[11]S. W. Lovesey and C. G. Windsor, J. Phys. Radium 32, 573 (1970).
[12]L. Van Hove, Phys. Rev. 95, 1374 (1954).
[13]See, for example, R. Peierls, *Quantum Theory of Solids* (Oxford U. P., Oxford, England, 1955), Sec. 4.2.
[14]D. F. Johnston, Proc. Phys. Soc. (London) 88, 37 (1966).
[15]A. R. Edmonds, *Angular Momentum in Quantum Mechanics* (Princeton U. P., Princeton, N. J., 1960), Sec. 2.5.
[16]R. Watson and A. Freeman, Acta Cryst. 14, 35 (1961).
[17]H. A. Mook, Phys. Rev. 148, 500 (1966).

PHYSICAL REVIEW B VOLUME 4, NUMBER 9 1 NOVEMBER 1971

Exciton Bands in Antiferromagnetic Cr_2O_3†

R. M. Macfarlane
IBM Research Laboratory, San Jose, California 95114

and

J. W. Allen
Lincoln Laboratory, Massachusetts Institute of Technology, Lexington, Massachusetts 02173

(Received 17 May 1971)

We have calculated the energy dispersion of the lowest eight ^2E Frenkel exciton branches in the four-sublattice antiferromagnet Cr_2O_3. This is the first such calculation for a magnetic insulator. The symmetry properties and $\vec{k}$ dependence of the interion exchange and Coulomb interactions which give rise to dispersion and Davydov splittings are presented in detail. Pairwise matrix elements of the interion Hamiltonian are treated as phenomenological parameters, and in most cases were determined from the $\vec{k}=0$ energies analyzed in an earlier paper. Dispersion curves for five directions in the rhombohedral Brillouin zone, and the exciton density of states, are given. Confirmation of the main features of the calculated exciton bands is provided by a measurement of the exciton-magnon absorption band shape. In the presence of a number of simplifying assumptions, this band shape is given by the joint exciton-magnon density of states. Good agreement between the calculated and observed band shape is obtained.

I. INTRODUCTION

Because of translational symmetry, the optical excitations within the localized electrons of magnetic insulators (usually $d \rightarrow d$ or $f \rightarrow f$ transitions) can properly be described as Frenkel excitons.[1] Coulomb and exchange interactions between the magnetic ions provide the mechanisms for the characteristic exciton properties, viz., Davydov splittings and dispersion. It is of considerable importance to establish the existence of these effects because they provide important insights into the